http://dx.doi.org/10.5516/NET.04.2013.078

ON-POWER DETECTION OF PIPE WALL-THINNED DEFECTS USING IR THERMOGRAPHY IN NPPS

JU HYUN KIM[1], KWAE HWAN YOO[1], MAN GYUN NA[1*], JIN WEON KIM[1], and KYEONG SUK KIM[2]
[1]Department of Nuclear Engineering, Chosun University
309 Pilmun-daero, Dong-gu, Gwangju 501-759, Republic of Korea
[2]Department of Mechanical Design Engineering, Chosun University
309 Pilmun-daero, Dong-gu, Gwangju 501-759, Republic of Korea
[*]Corresponding author. E-mail : magyna@chosun.ac.kr

Received August 20, 2013
Accepted for Publication October 21, 2013

Wall-thinned defects caused by accelerated corrosion due to fluid flow in the inner pipe appear in many structures of the secondary systems in nuclear power plants (NPPs) and are a major factor in degrading the integrity of pipes. Wall-thinned defects need to be managed not only when the NPP is under maintenance but also when the NPP is in normal operation. To this end, a test technique was developed in this study to detect such wall-thinned defects based on the temperature difference on the surface of a hot pipe using infrared (IR) thermography and a cooling device. Finite element analysis (FEA) was conducted to examine the tendency and experimental conditions for the cooling experiment. Based on the FEA results, the equipment was configured before the cooling experiment was conducted. The IR camera was then used to detect defects in the inner pipe of the pipe specimen that had artificially induced defects. The IR thermography developed in this study is expected to help resolve the issues related to the limitations of non-destructive inspection techniques that are currently conducted for NPP secondary systems and is expected to be very useful on the NPPs site.

KEYWORDS : IR Thermography, Wall-thinned Defects, IR Camera, Cooling Device, Finite Element Analysis (FEA), On-power Inspection

1. INTRODUCTION

The number of aging nuclear power plants (NPPs) has increased recently. Accordingly, the number of operational interruptions has increased due to malfunctions of the NPPs secondary systems. These cases occur in the secondary systems of NPPs with a range of structures due to fatigue, wall-thinned defects, corrosion, etc. Of these problems, wall thinned defects occur in the pipes by the diffusion of the corrosion with the flow of the fluids, and the defects frequently take place in carbon steel pipes with lower Cr content. Such wall-thinned defects can lead to damage without warning signs and they can be found frequently in the base material part. Therefore, they are one of the major factors that degrade the integrity of a pipe [1], [2].

Systematic management of wall-thinned defects requires regular inspections. In particular, systematic management requires a close inspection even when the NPP is in normal operation. The secondary system of a NPP is the place to which the operators or workers gain access for their work frequently. Unexpected damage to a pipe may have significant social impacts, which highlights the importance of systematic management of wall-thinned defects. Consequently, considerable attention has been paid to non-destructive inspections to examine the integrity of major facilities. In addition, there is increasing demand for non-destructive inspection methods that are relatively safe and enable measurement in a quick and easy manner [3].

Currently, a range of non-destructive inspections are conducted, such as ultrasonic testing (UT), eddy current testing (ECT), and magnetic particle testing (MT) [4], [5]. Non-destructive inspection techniques involve infrared (IR) thermography. IR thermography is expected to help resolve the issues related to the limitations of the existing non-destructive inspection techniques because it is used to examine defects based on measurements of the temperature difference between defective parts and non-defective parts. IR thermography is also expected to be useful on a NPP site [6].

IR thermography with a cooling device is a reliable technique for detecting wall-thinned defects in the inner pipes of NPPs that are in normal operation, and is expected to facilitate the maintenance of secondary systems of NPPs. The results of this study will be used as the basic material for the inspection of wall-thinned defects.

2. THEORETICAL BACKGROUND

2.1 IR Thermography

When a specific target is cooled from an outside cooler, thermal diffusion is disturbed on the surface of the target depending on the existence of defects inside the target. In this case, the insulation effect by defects inside the target induces temperature differences on the target surface. IR thermography is used to measure the temperature of the surface of the target and convert the measurement results to an image in real time. Based on a real-time image obtained using an IR camera, it is possible to measure the shape and location of the defects inside the target [7].

IR thermography has the following features [8]:
- Non-contact technique
- Full-field image of stress
- Energy measurement technique
- Easy visual interpretation of the results

Currently, IR thermography has been applied to the military field, stress analysis, welding monitoring, evaluation of heat transfer characteristics, deterioration diagnosis of power facilities, defect inspection in composites, and medical diagnosis [9]. Fig. 1 shows the principle of IR thermography.

2.2 Theory

All objects have a temperature that is above absolute zero and they emit radiant energy that corresponds to their temperature [10].

$$\frac{dR(\lambda,T)}{d\lambda}=\frac{2\pi hc^2\lambda^{-5}}{e^{hc/\lambda kT}-1}, \quad (1)$$

where

Plank's constant $h = 6.626\times10^{-34} J\cdot s$
Boltzmann's constant $k = 1.380546\times10^{-23}$
Speed of light $c = 2.998\times10^{8} ms^{-1}$.

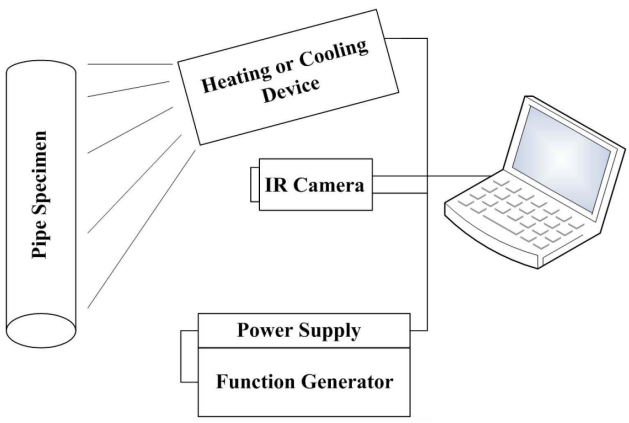

Fig. 1. Diagram of IR Thermography.

Eq. (1) describes Plank's theory of black body radiation. According to the theory, there is a simple relationship between the characteristics of black body radiation (energy intensity, R, and wavelength, λ) and its temperature, T. Moreover, the amount of radiation emitted from a black body radiator per unit time is determined only by temperature. The characteristics can be used to calculate the temperature of the black body. IR thermography provides a temperature image using the correlation between temperature and detected energy [10]. The integration of Eq. (1) over the total wavelength range $\lambda = 0$ to $\lambda = \infty$ gives:

$$R=\sigma T^4, \quad (2)$$

where

Stefan-Boltzmann's constant $\sigma = 5.67\times10^{-8} W/(m^2\cdot K^2)$.

Eq. (2) describes Stefan-Boltzmann's law. This theory states that the total energy radiated per unit surface area of a black body and per unit time is directly proportional to the fourth power of the absolute temperature, T. In this case, T represents the absolute temperature in Kelvin of an object and R_t is the reflection intensity of a black body. The IR camera can measure the temperature using Eqs. (1) and (2) [10].

An ideal black body emitter does not exist in reality. If the energy emitted from a real object is R_a and the energy emitted from a black body is R_b, the emissivity which is the ratio of energy radiated by an object to energy radiated by a black body at the same temperature can be expressed by Eq. (3) [10].

$$\varepsilon=\frac{R_a}{R_b} \quad (3)$$

In this case, if ε =1, the object is called a black body. Therefore, for metal with low emissivity, the emissivity can be kept at 0.95 if a black matte color spray is applied, which is close to a black body.

3. OPTIMAL COOLING METHOD

In an NPP that is in normal operation, the pipes are covered with insulators and are at high temperature, transferring heat to the surface of the insulators. The thermal conduction in the specimen is related with the following equation where the heat flux is equal to the product of the thermal conductivity, k, and the negative temperature gradient, $-\nabla T$:

$$q=-k\nabla T \quad (4)$$

When a cooling device is used to cool the pipes at high temperatures, thermal diffusion is disturbed depending on the existence of defects inside the pipes. Insulation effects by defects induce local differences in temperature

on the surface of the pipes. When an IR camera is used to obtain a thermal image of the pipes, where such a temperature difference occurs, defects in the pipes are shown in the image. Therefore, in this study, an optimal cooling method was selected to obtain an IR image of defects in a geometric shape in an easier and quicker way with a view to examine the defect size and depth from the surface. Cooling methods include using a water-cooled air cooler or an air-cooled air cooler, a tube air cooler, a heat pipe-type cooler, and a fan cooler. Table 1 lists the characteristics of these cooling methods.

As shown in Table 1, the cooling method using a fan was evaluated to be the best among the various cooling methods. The fan cooling method can be combined with other cooling methods or can be used independently. Therefore, the fan cooling method was used in this study to detect wall-thinned defects inside the pipe based on IR thermography.

4. SIMULATIONS AND EXPERIMENTS

In this study, the fan-type cooling device was selected as the method for cooling a pipe specimen. Before the experiments, finite element analysis (FEA) was conducted to examine the cooling effect of the selected cooling device as well as the optimal experiment conditions. FEA was performed using ANSYS FLUENT 13.0, and the GAMBIT program was used to generate the meshes that were modeled to conduct FEA [11], [12]. In addition, based on the FEA results, cooling experiments were performed to detect defects inside the pipe specimen.

4.1 Specimen and Equipment

The pipe specimen used in this study has defects inside. The pipe specimen constructed for the experiments was made of Shc.80 ASTM A106 Gr.B, which is similar to the actual pipes used in NPPs. As shown in Fig. 2, the

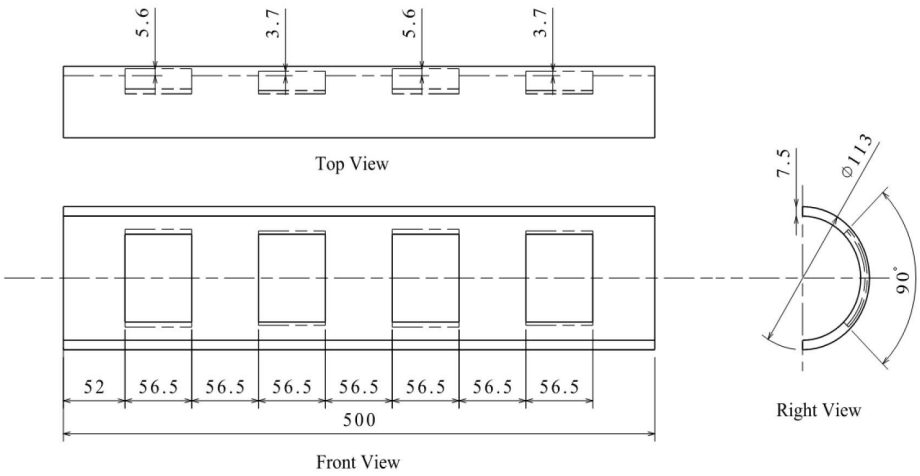

Fig. 2. Design of a Pipe Specimen.

Table 1. Applicability of the Cooling Methods

Cooling method	Applicability
Air tube cooler	As compressed air is used for cooling, the cooler is cheap and portable. The cooler has low capacity, which is effective for cooling locally. On the other hand, it requires additional equipment to use compressed air. Some limitations are expected when a cooler is used on the site of NPPs.
Air-cooled air cooler and water-cooled air cooler	The coolers enable the maintenance of a constant temperature and can be adjusted over a wide range of use. They show excellent cooling capability with high efficiency. On the other hand, the initial manufacturing cost is high. They are heavy and unsuitable for portable use.
Heat pipe-type cooler	The cooler has high cooling efficiency while the water quantity in a heat pipe can be adjusted, which enables manufacture in a range of forms. In addition, the interval of the heat pipe itself can be adjusted. On the other hand, the cooler shows high cooling efficiency when it is installed directly on the target. A fan also needs to be installed.
Fan cooler	A fan is readily available, and its wings can be manufactured in a variety of forms. The angle of the cooler can be adjusted while the rotation speed of the fan can be adjusted continuously and freely. In addition, the cooler can be manufactured to be light weight. Therefore, it is believed that the cooler will be easy to use and portable.

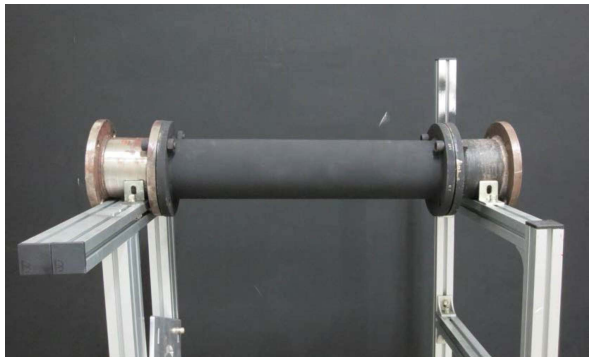

Fig. 3. Pipe Specimen.

Table 2. Dimensions of the Defects in the Pipe Specimen

	Size
Circ. Angle. θ/π	0.25
Depth. d/t	0.5, 0.75
Length. L/D_0	0.5

pipe specimen has a total length of 500mm, thickness of 7.5mm, 4 inches in diameter, and external diameter of 113mm. On the inner surface, four defects were created of a constant length. Two of the defects had a depth of 50% and the other two had a depth of 75% of the thickness of the pipe specimen. Table 2 lists the shape of each defect. A black matte color spray was also applied to the surface of the pipe specimen to maintain a surface emissivity of 0.95 and minimize the reflection of light. Fig. 3 shows the pipe specimen that was manufactured in this study.

A blower fan was used as a cooling device to cool the pipe specimen. The blower fan had 6 wings with a maximum wind speed of 16.5m/s. The size of its wing was 27cm. The blower fan allows uniform cooling of the pipe specimen.

4.2 Numerical Simulation

In regard to experiments for wall-thinned defects inside the pipe, thermal analysis can be performed based on the FEA prior to experiments. The FEA provides the data to predict problems in the thermal distribution of the pipe specimen based on an analysis of the simulation results, to configure the cooling device that can be applied to an actual environment, and investigate the optimal experiment conditions.

In this study, the pipe specimen used for the experiment was ASTM A106 Gr.B, which is frequently used for actual pipes of the NPP's secondary system that was manufactured from carbon steel. Therefore, pipe modeling for FEA was performed under the same conditions as those for the pipe specimen that was used for the experiment on the cooling devices.

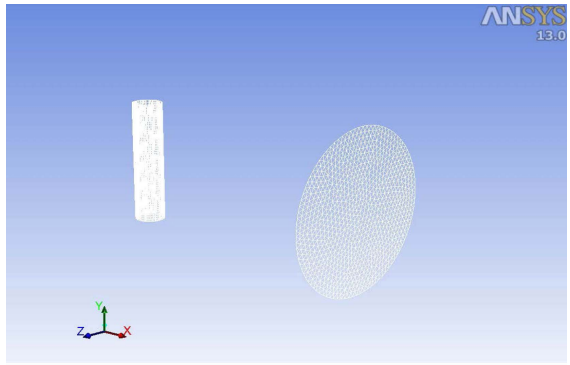

(a) Diagram of the pipe model and fan model

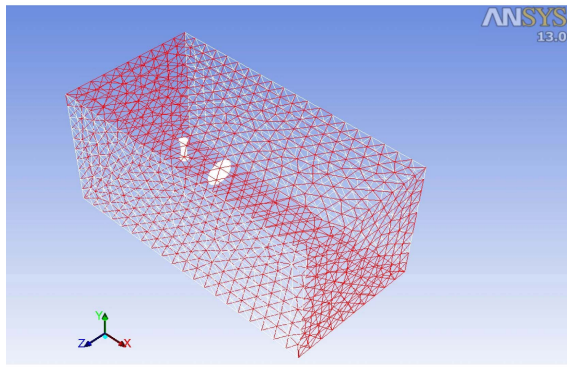

(b) Creation of meshes

Fig. 4. Configuration of the Modeled Pipe Specimen and Fan.

This study used a cooling device based on the principles of a fan. Therefore, to conduct an FEA of the cooling device, the principles of a fan were applied to cool the pipe model through forced convection caused by the pressure difference between the surfaces of the fan model and the pipe model. In addition, water was designed to flow inside the pipe model to describe a hot pipe in the NPP in normal operation. The mass flow rate of water was set to 1kg/sec. Fig. 4 (a) shows diagrams of the pipe model and fan model. Fig. 4 (b) shows the meshes that were created to improve the analysis accuracy. ANSYS FLUENT was used to perform a simulation of the FEA for a cooling device [11]. The distance between the fan model and pipe model and the pressure difference in the fan model were adjusted. For simulation conditions, the distance between the pipe model and the fan model was adjusted to 1m, 2m, and 3m, whereas the pressure difference in the fan model was set to 100Pa and 150Pa. The temperature of water flowing inside the pipe model was adjusted to 150 °C and 200 °C. Here, the pressure difference of 100Pa can be represented by 12.4 m/s and the pressure difference of 150 Pa can be represented by 15.2 m/s.

The basic boundary conditions for the FEA were established as follows. To simplify the analysis, symmetric conditions were set to consider half of the pipe model. In

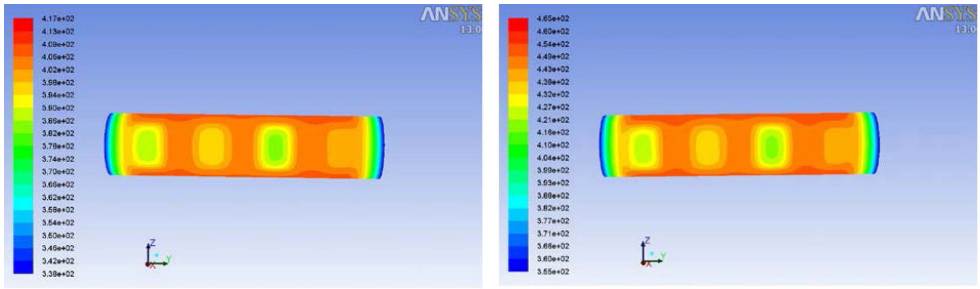

(a) 150 °C (423.15 °K), 1m

(d) 200 °C (473.15 °K), 1m

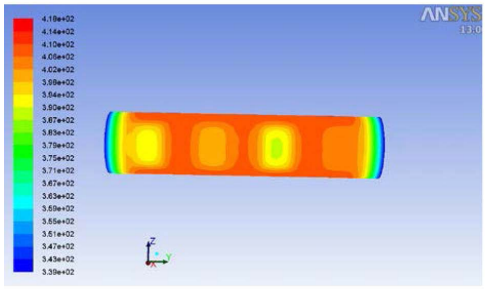

(b) 150 °C (423.15 °K), 2m

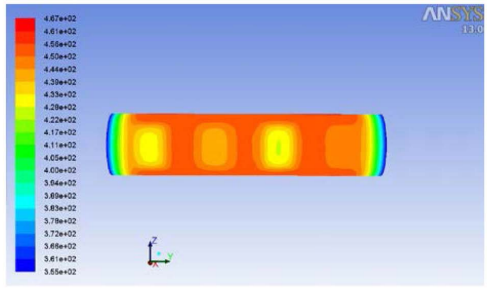

(e) 200 °C (473.15 °K), 2m

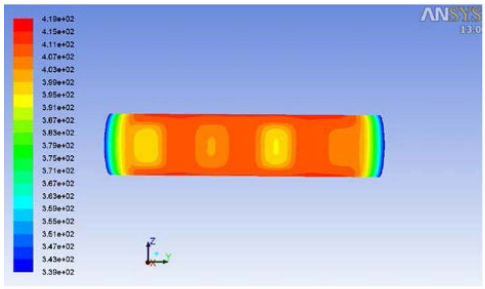

(c) 150 °C (423.15 °K), 3m

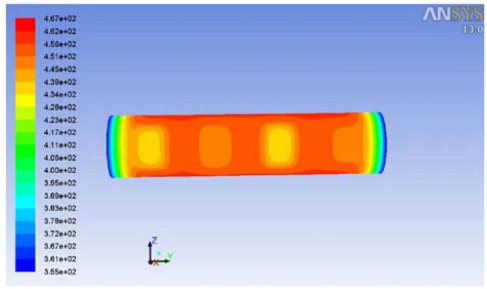

(e) 200 °C (473.15 °K), 3m

Fig. 5. Pressure Difference of 100 Pa in the Fan Model.

addition, the temperature (25 °C) and humidity for the entire space were kept constant, excluding those for the pipe model and cooling device model.

4.3 Simulation Results

The simulation results were taken based on the image at 30 seconds, which showed the defects most clearly compared to the simulation results that were conducted for 60 seconds. Fig. 5 shows the simulation results obtained when the surface pressure difference between the fan model and pipe model was 100Pa, the temperature of the pipe model was 150 °C and 200 °C, and the distance between the pipe model and fan model was adjusted to 1m, 2m, and 3m. The deviation of temperature in the defect parts was conspicuous under all simulation conditions regardless of the distance between the pipe model and fan model. In addition, Fig. 6 shows the simulation results obtained when the surface pressure difference between the fan model and pipe model was 150Pa, the temperature of the pipe model was 150 °C and 200 °C, and the distance between the pipe model and fan model was adjusted to 1m, 2m, and 3m. The shape of the defects was observable with the naked eye. The defects appeared clearer as the pressure difference in the fan model increased regardless of the depth of the defects. Moreover, the defects became more distinct when the distance between the pipe model and fan model was shorter (1m and 2m).

Consequently, the FEA could confirm the cooling effects of the fan cooling device. The optimal experiment conditions include a pressure difference of 150Pa in the fan and a close distance, such as 1m or 2m, between the pipe specimen and fan cooling device.

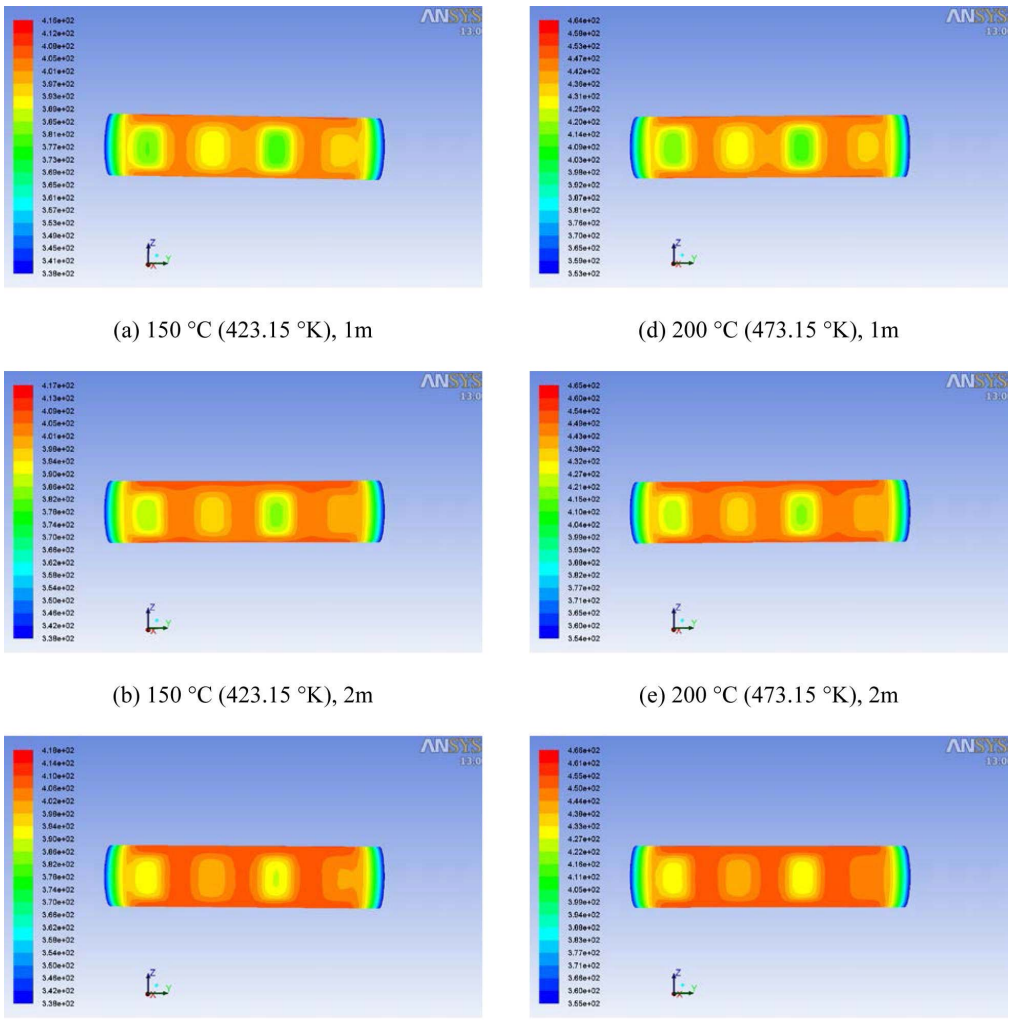

(a) 150 °C (423.15 °K), 1m

(d) 200 °C (473.15 °K), 1m

(b) 150 °C (423.15 °K), 2m

(e) 200 °C (473.15 °K), 2m

(c) 150 °C (423.15 °K), 3m

(f) 200 °C (473.15 °K), 3m

Fig. 6. Pressure Difference of 150 Pa in the Fan Model.

4.4 Experiments

The FEA that was conducted based on the numerical technique before the experiment could confirm the cooling effects of the cooling device. In this study, an IR camera and a cooling device were configured according to the experiment conditions established based on the FEA.

The temperature of the pipe should be kept high because it is assumed that inspections are conducted for wall-thinned defects inside the pipes of the NPPs that are in normal operation. To this end, a heating device in the pipe was manufactured. The inner heating device was manufactured to ensure that the support was close to the inner wall of the pipe specimen and the support could be wrapped up with two heating tapes that could be heated up to 400 °C. Fig. 7 shows the inner heating device used to implement a hot pipe.

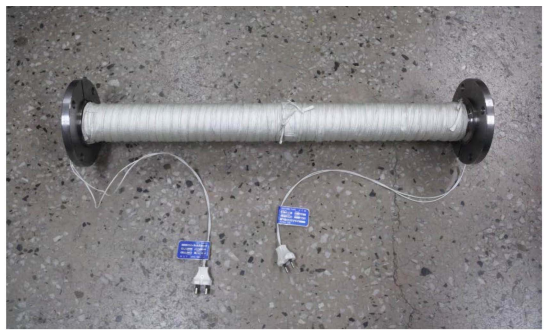

Fig. 7. Inner Heating Device for the Pipe Specimen.

To verify the heating performance of the inner heating device, the device was installed inside the pipe specimen before being heated up. An IR camera was used to measure

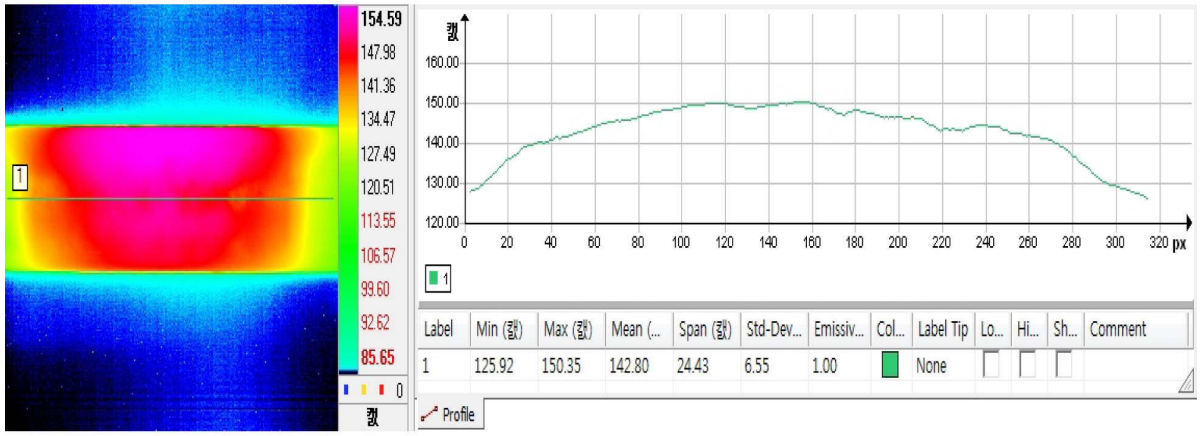

Fig. 8. Temperature Distribution of the Inner Heating Device.

Fig. 9. Experimental Equipment Using the Cooling Device.

the temperature distribution. The measurement results showed that the surface temperature of the 4-inch pipe specimen was kept at 142.0 °C ~150.35 °C depending on the location when the temperature of the two heating tapes was set at 320.0 °C each. Fig. 8 shows the surface temperature of the pipe specimen that was measured using an IR camera when the maximum surface temperature of the pipe specimen was approximately 150 °C. According to the measurement results, the highest temperature was observed in the center of the pipe specimen. The temperature tended to decrease with increasing distance from the center. The low temperature of both edges was expected from the relatively large heat loss caused by the flange parts of both pipe ends.

Fig. 9 shows how the authors configured the experimental equipment, including an IR camera, a fan, a pipe specimen, heating tape, a heating tape controller, and a PC, for the detection of wall-thinned defects inside the pipe. The experiment was conducted in a closed space while the temperature in the laboratory was kept constant at 25 °C using an air conditioner.

Table 3. Measured Wind Speed at the Surface of the Specimen

Distance from the specimen to the cooling device	One fan	Two fans
1m	10.8m/s	12.6m/s
2m	6.69m/s	8.6m/s

To emulate a pipe of the NPPs that was under normal operation, the inner heating device was used to maintain the temperature of the pipe specimen at 150 °C, whereas the distance between the pipe specimen and the fan, and the number of fans changed. The distance between the pipe specimen and the IR camera was fixed to 1m, whereas the distance between the pipe specimen and fan was adjusted to 1m and 2m. In addition, the number of fans was adjusted to 1 and 2 and each experiment was conducted for 120 seconds. The measured wind speeds at the surface of the specimen are given in Table 3.

4.5 Experiment Results

Fig. 10 (a) and Fig. 10 (b) show the experiment results when a single fan was used with a distance between the pipe specimen and the fan adjusted to 1m and 2m, respectively. The defects created up to 75% and 50% depths inside the pipe specimen were detected at a distance of 2m. The defects were detected more clearly as the distance between the pipe specimen and fan became shorter. Also, because of a large cooling effect at the flange parts of both pipe ends, two defects near the flange parts were not detected but two defects in the center were detected. Fig. 10 (c) and Fig. 10 (d) show the experimental results when two fans were used to cool the pipe specimen at a distance of

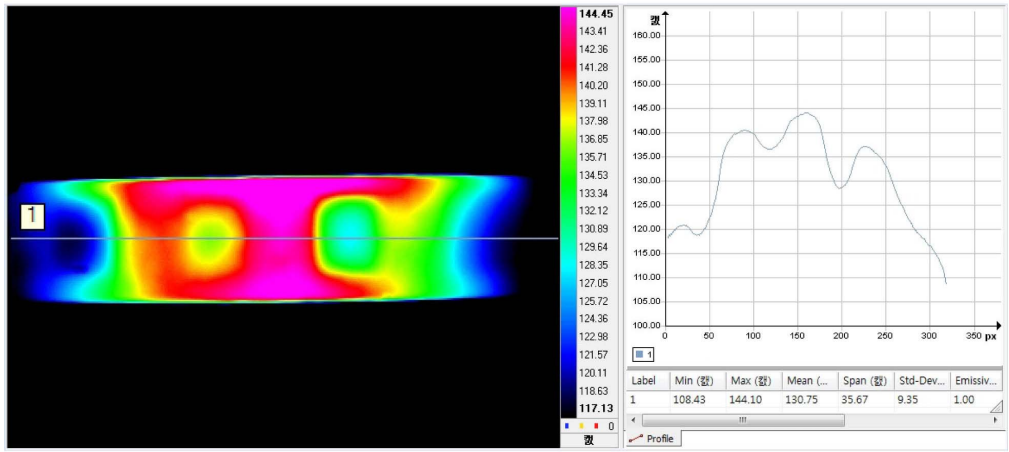

(a) One fan (distance 1m)

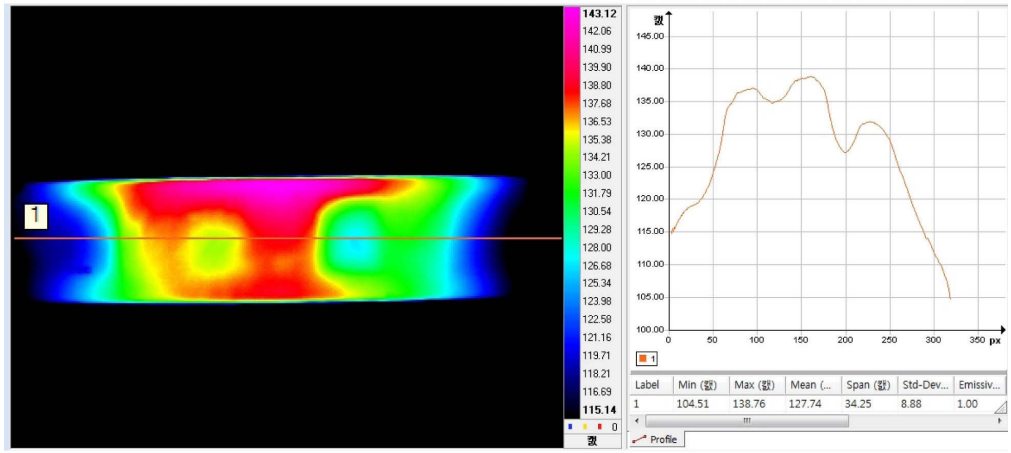

(b) One fan (distance 2m)

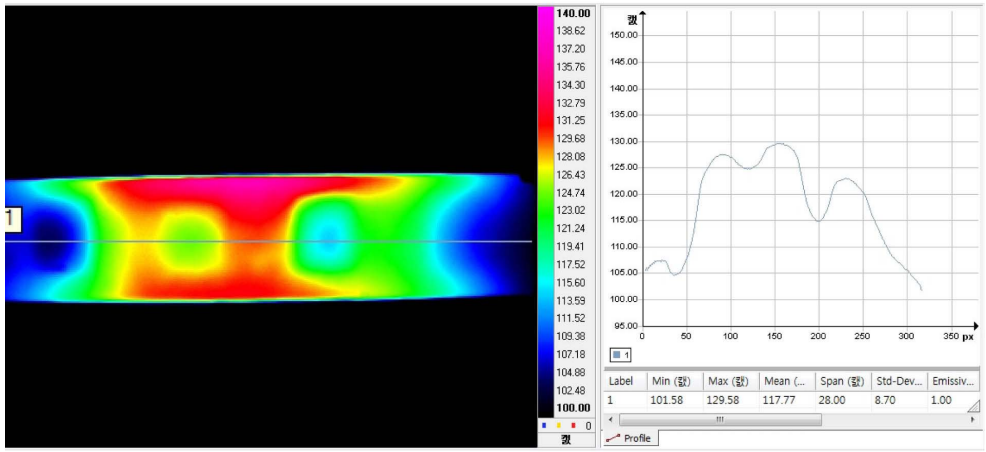

(c) Two fans (distance 1m)

Fig. 10. Experiment Results.

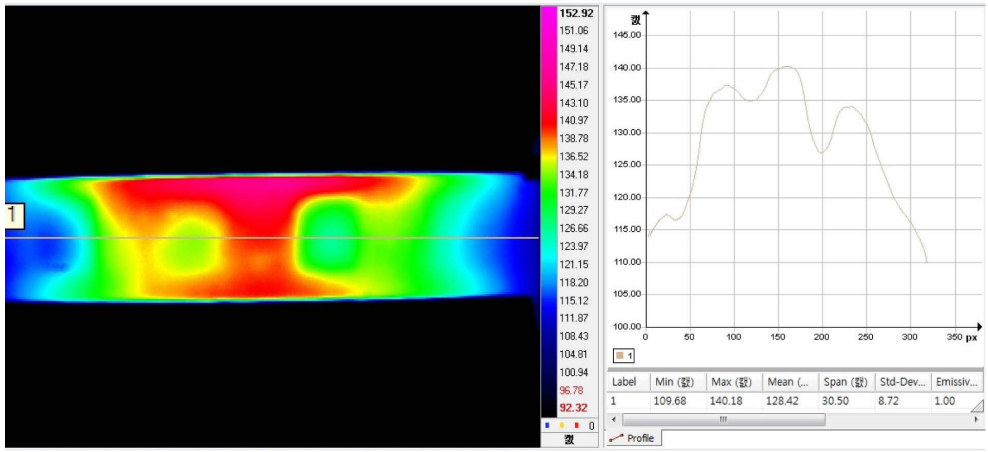

(d) Two fans (distance 2m)

Fig. 10. Experiment Results.

1m and 2m, respectively. According to the experiment results, the defects that were created artificially with 75% and 50% depths inside the pipe specimen could be detected. The defects were detected more conspicuously as the distance between the pipe specimen and cooling device became shorter. In particular, two defects of the central portion and one defect of the left flange portion could have been detected at all distances. The other was not detected because the depth of the defect was thin and the cooling at the right flange had an effect on the rightmost defect detection.

5. CONCLUSIONS

In this study, IR thermography was used to detect wall-thinned defects inside the pipes of NPPs that were in normal operation. A pipe model and pipe specimen with the same physical properties as those for the actual pipes of NPPs was used for the FEAs and the experiments. Moreover, the sizes of the defects applied to the pipe specimen were equal to those of the defects applied to the pipe model for the FEA.

The FEA was conducted to examine the cooling effects of a cooling device and the optimal experiment conditions. The results predicted that the detectability of defects increased with decreasing distance between the pipe and fan, and increasing wind speed of the fan. The results of the FEA were applied to subsequent experiments.

Three defects could be detected partially in the experiment that was conducted using the cooling fans based on the FEA. A little differently from the FEA results, the defects could be detected clearly when the distance between the pipe specimen and fan was 1m and two cooling devices were used. To detect wall-thinned defects in the NPP that is in normal operation based on such results, the distance between the pipe and fan should be short (e.g. 1m), whereas the wind speed and air flow of the fan should be high.

In conclusion, IR thermography enabled the detection of wall-thinned defects inside the pipe and is expected to be quite useful on the NPP site compared to the existing non-destructive inspection. Moreover, because IR thermography facilitates the maintenance of facilities of the NPPs that are in normal operation, it is expected to maximize the operation efficiency of NPP facilities and minimize the energy loss and economic loss that can be attributed to operation stoppage.

ACKNOWLEDGEMENT

This work was financially supported by the nuclear research and development program of the Korea Institute of Energy Technology Evaluation and Planning (KETEP) grant funded by the Ministry of Trade, Industry and Energy, the Republic of Korea.

REFERENCES

[1] M. Frank, R. Hans, and S. Helmut, "Experience with piping in German NPPs with Respect to Ageing-Related Aspects," *Nucl. Eng. & Des*., vol. 207, pp. 307-316 (2001).
[2] K. S. Kim, H. S. Chang, D. P. Hong, C. J. Park, S. W. Na, K. S. Kim, and H. C. Jung, "Defect Detection of the Wall Thinning Pipe of the Nuclear Power Plant Using Infrared Thermography," *Journal of the Korean Society for Nondestructive Testing*, vol. 30, pp. 85-90 (2010).
[3] G. Shen and T. Li, "Infrared thermography for high-temperature pressure pipe," *Insight*, vol. 49, pp. 151-153 (2007).
[4] P. K. Rastogi and D. Inaudi, "Trends in Optical Nondestructive Testing and Inspection," Elsevier Science (2000).
[5] C. J. Hellier, "Handbook of nondestructive evaluation," McGraw-Hill, 2nd Ed. (2001).
[6] A. Vageswar, K. Balasubramanian, C. V. Krishnamurthy,

T. Jayakumar, and B. Raj, "Periscope infrared thermography for local wall thinning in tubes," *NDT&E International*, vol. 42, pp. 275-282 (2009).
[7] J. M. Lloyd, "Thermal Imaging Systems," Plenum press (1979).
[8] S. V. Patankar, "Numerical Heat Transfer and Fluid Flow," Hemisphere Pub. Co. (1980).
[9] H. D. Lee, "Thermal measurement theory using infrared camera," *Journal of KSNVE*, vol. 17, pp. 31-34 (2007).
[10] X. P. V. Maldague and P. O. Moore, "Nondestructive Testing Handbook: Infrared and Thermal Testing," *American Society for Nondestructive Testing*, vol. 3, 3rd Ed., pp. 223-246 (2001).
[11] ANSYS, ANSYS 13.0 (Release 13.0), ANSYS Inc. (2010).
[12] Fluent, GAMBIT 2.1, Fluent Inc. (2003).